Spatially modulated photoluminescence properties in dynamically strained GaAs/AlAs quantum wells by surface acoustic wave

Tetsuomi Sogawa,[1,a)] Haruki Sanada,[1] Hideki Gotoh,[1] Hiroshi Yamaguchi,[1] and Paulo V. Santos[2]
[1]*NTT Basic Research Laboratories, NTT Corporation, 3-1 Morinosato-Wakamiya, Atsugi, Kanagawa 243-0198, Japan*
[2]*Paul Drude Institute, Hausvogteiplatz 5-7, 10117 Berlin, Germany*

(Received 5 November 2011; accepted 27 March 2012; published online 20 April 2012)

Spatially resolved photoluminescence (PL) spectra and polarization anisotropy were investigated in GaAs/AlAs dynamic wires, which were formed by applying a surface acoustic wave (SAW) on GaAs/AlAs quantum wells along the [110] or [1-10] direction. A synchronized excitation method clearly demonstrates that the band gap energies are spatially modulated by the travelling-SAW-induced strain. It is found that both the spatial PL modulation and anisotropic polarization properties depend on the SAW direction. The spatial modulation of the polarization anisotropies and their dependence on the strain-induced valence band mixing are also discussed theoretically. © *2012 American Institute of Physics*. [http://dx.doi.org/10.1063/1.3703309]

The quantum confinement of carriers in artificial semiconductor structures has contributed both to fundamental scientific studies and to the development of electrical and optical devices.[1] In particular, basic physical properties such as the electronic band gap and the strength of excitonic transitions can be controlled in quantum well (QW) structures by using sophisticated epitaxial growth techniques based on the static control of material composition and dimensions. Surface acoustic waves (SAWs) are known to provide a dynamic lateral modulation of the band structure of QWs while avoiding the deleterious effects introduced by fabrication processes.[2–10] Furthermore, the band modulation introduced by SAWs differs qualitatively from that induced by a static modulation, because its time and spatial dependence allow for the dynamic control of the material properties.[9,10] In fact, unique dynamic properties have been reported including photoluminescence (PL) quenching due to the lateral piezoelectric field and subsequent recombination of the separated carriers after the macroscopic transport,[3] the polarization anisotropy of PL spectra caused by strain-induced band mixing,[5,10] and spin manipulation capability.[11–14]

We investigated both the spatial-dependent PL spectra and polarization anisotropy in GaAs/AlAs dynamic wires (DWRs) formed by applying a SAW along the [110] or [1-10] direction of GaAs/AlAs (001) QWs. Previous studies using a cw excitation method, which investigated the time-averaged spectra of the travelling DWRs, reported that each excitonic PL line splits into two peaks due to the strain-induced band gap modulation and that the relative intensity of the split peaks changes with the SAW propagation direction.[5–7] The crystal orientation dependence of the PL modulation was explained by the different capture efficiencies of electrons, which are determined by the relative phase between the strain-induced band gap modulation and the piezoelectric modulation.[6] In this study, we adopted a synchronized excitation method[15] to clarify directly the relationship between the SAW phase and the spatial PL modulation. We demonstrated that PL peaks corresponding to the minima and maxima of the band gap modulation alternately appear with a SAW phase difference of π. We also showed that both the spatial PL modulation and the anisotropic polarization properties depend on the SAW direction. The dynamic polarization anisotropies and their dependences on depth and in-plane position were theoretically analyzed and were in good agreement with the experimental findings.

In the experiment, we used high quality GaAs/AlAs QWs with various well thicknesses ($L_z = 6.3$, 7.1, 8.3, 9.9, 12.2, 15.2, 19.8, and 83 nm), which were grown by molecular beam epitaxy on a GaAs (001) substrate. Each QW was separated from the others by AlAs(2.0 nm)/GaAs(2.0 nm) superlattice barrier layers with a total thickness of 26 nm. The QWs were located between 100 and 400 nm from the surface, on which inter-digital transducers (IDTs) were deposited to generate SAWs propagating along the [110] and [1-10] directions. As the SAW frequency was 820 MHz, the SAW wavelength (λ_{SAW}) corresponds to approximately 3.6 μm, assuming a SAW phase velocity of 2950 m/s. Mode-locked pulses (1.5 ps, 82 MHz, 720 nm, and 15-20 μW) from a Ti-sapphire laser synchronized with the SAW frequency were used to generate carriers, i.e., delivering one optical excitation pulse for every 10 SAW periods. Low temperature (4 K) spatially resolved PL spectra were measured in a helium gas-flow cryostat using a confocal micro-PL setup with a spatial resolution of approximately 1 μm. The PL was spectrally analyzed by using a spectrometer connected to a charge-coupled device (CCD) detector. The SAW linear power density P_l per beam (defined as the acoustic power flux per unit length along the cross-section of the SAW beam) was in the 100 to 200 W/m range as estimated from a comparison of the observed band gap energy shifts in the PL spectra and the theoretical values.[5]

A single SAW spatially modulates both the piezoelectric potential Φ_{SAW} and the band gap energy on the QW plane. The schematic illustrations of Figs. 1(a) and 1(b) compare

[a)]E-mail: sogawa.tetsuomi@lab.ntt.co.jp.

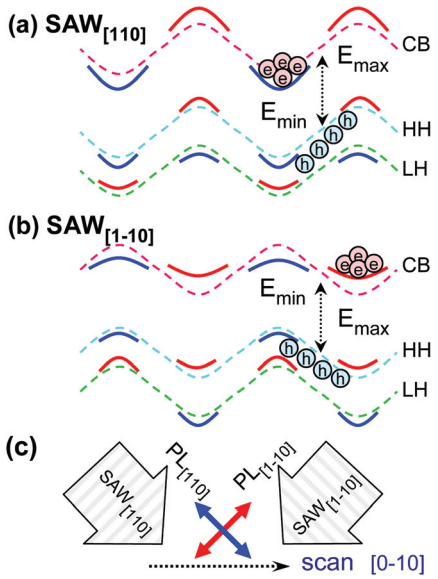

FIG. 1. (a) Schematic illustration of the changes in the band structures for $SAW_{[110]}$ and (b) for $SAW_{[1-10]}$. (c) The SAW propagation direction is rotated by 45° with respect to the optical setup.

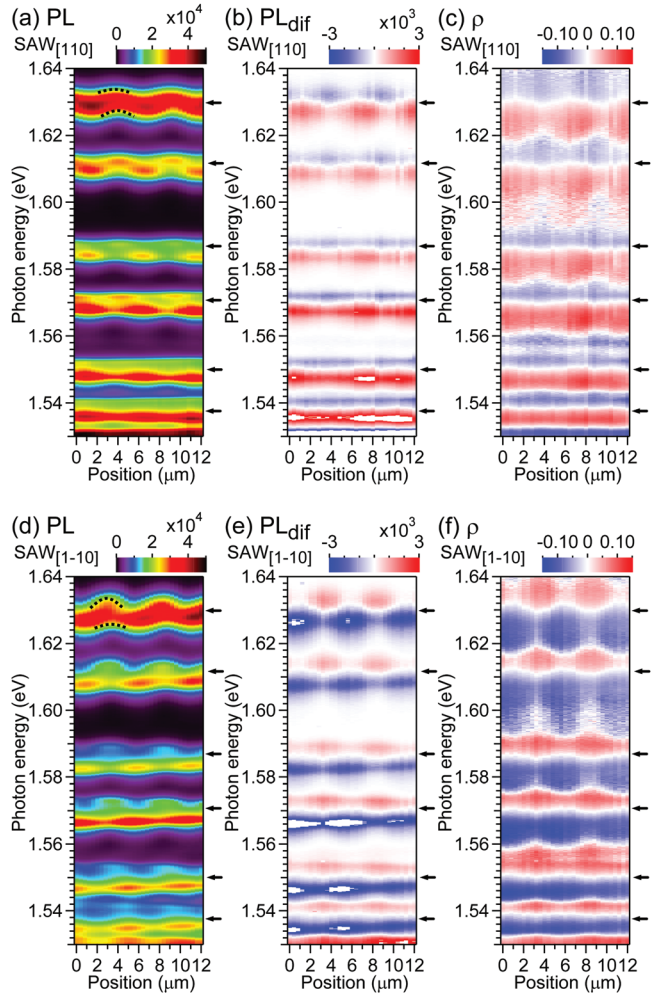

FIG. 2. (a) Spatially resolved PL spectra, (b) PL_{dif} spectra, and (c) ρ spectra for $SAW_{[110]}$, where arrows indicate the excitonic transition energies for each QW in the absence of a SAW. (d) Spatially resolved PL spectra, (e) PL_{dif} spectra, and (f) ρ spectra for $SAW_{[1-10]}$.

the changes in the band structure induced by the SAW along the [110] ($SAW_{[110]}$) and along [1-10] ($SAW_{[1-10]}$) directions, respectively. Dashed lines show the modulation of the electronic energy ($-q\Phi_{SAW}$) for the conduction band (CB), heavy-hole band (HH), and light-hole band (LH), while solid lines, which are exaggerated compared with the scale for the dashed lines, represent their corresponding energy shifts. Note that the energy shift is of opposite sign for HH and LH. E_{max} (E_{min}) denotes the positions where the band gap energy between the CB-HH transition is a maximum (minimum) due to the compressive (tensile) hydrostatic strain ϵ_{hydro}. The D_{4d} symmetry of the GaAs lattice gives rise to Φ_{SAW} of opposite signs for SAWs along the [110] and [1-10] directions.[6] It was reported that the energy shifts vary with the depth from the surface.[13] In the PL polarization studies, the preferential polarization directions of the sample, i.e., [110] and [1-10], are rotated by 45° with respect to the horizontal and vertical axes of the optical setup, as shown in Fig. 1(c). Here, $SAW_{[110]}$ ($SAW_{[1-10]}$) travels from top left to bottom right (top right to bottom left). This configuration minimizes effects associated with the residual polarization properties of the setup. Spatially resolved PL measurements were carried out by scanning the sample stage along the [0-10] direction with a step of 0.4 μm. We define the PL difference (PL_{dif}) and the degree of polarization anisotropy (ρ) as $(PL_{[1-10]} - PL_{[110]})$ and $(PL_{[1-10]} - PL_{[110]})/(PL_{[1-10]} + PL_{[110]})$, respectively, where $PL_{[1-10]}$ ($PL_{[110]}$) represents the PL intensity polarized parallel to the [1-10] ([110]) direction.

Figures 2(a) and 2(d) compare the spatially resolved PL spectra for $SAW_{[110]}$ and $SAW_{[1-10]}$, respectively, where the arrows indicate the excitonic transition energies for each QW in the absence of a SAW. We found that the emission from each QW, which should be single peaked without a SAW, oscillates between the values E_{min} and E_{max}. It should be noted that the intensities of these emissions at the photon energies of E_{min} and E_{max} alter periodically with opposite phases as the position is scanned. Since the scan axis is rotated by 45° with respect to the SAW propagation direction, the observed modulation period of 5.1-5.4 μm corresponds to $\sqrt{2}\lambda_{SAW}$. Figure 2 demonstrates that the strain-induced band gap modulation and the piezoelectric modulation as generated by the SAW create multiple vertically stacked lateral wires with widths determined by half λ_{SAW} of approximately 1.8 μm. In Figs. 2(a) and 2(d), dotted lines represent the contour lines of the PL intensity near the E_{max} site (position of 3-4 μm) for the 6.3 nm QW (centered at approximately 1.63 eV). The curvature of the contour lines in the higher-energy side is larger for $SAW_{[1-10]}$ than that for $SAW_{[110]}$, while the contour lines in the lower-energy side show an opposite tendency. These differences are attributed to the carrier dynamics driven by the piezoelectric field. In general, electrons can quickly move to electron-attractive sites, i.e., minima of $-q\Phi_{SAW}$, due to the high electron mobility, as illustrated in Figs. 1(a) and 1(b), where electrons and holes are assumed to be photo-excited at the center of E_{max} and E_{min} positions. In contrast, holes will stay near the photo-excitation position, which is much broadened than the laser spot due to the initial diffusion of hot carriers, irrespective of the piezoelectric field because of their relatively low mobility. Thus, the efficiency of exciton formation is

enhanced when carriers are excited at the E_{min} (E_{max}) sites for $SAW_{[110]}$ ($SAW_{[1\text{-}10]}$).

The spatially resolved PL_{dif} (ρ) spectra for $SAW_{[110]}$ and $SAW_{[1\text{-}10]}$ are shown in Figs. 2(b) and 2(e) (Figs. 2(c) and 2(f)), where the red and blue signals correspond to the polarization parallel to the [1-10] and [110] direction, respectively. It is demonstrated that ρ changes its sign between the lower and higher energy sides of each PL line in the absence of a SAW (indicated by the arrows), and that the preferential polarization direction in the lower (higher) energy side is perpendicular (parallel) to the SAW propagation direction for both SAWs.

To provide a theoretical discussion, we have analyzed the spatial dependences of the SAW-induced energy shifts of the CB, HH, and LH as well as the transition matrix elements based on a calculation of the displacement field of the Rayleigh SAW wave including the piezoelectric coupling.[5,16] Figure 3(a) shows the spatial distribution of ϵ_{hydro} as functions of a depth and an in-plane position, which are normalized by λ_{SAW}. Figures 3(b)–3(d) show the spatial distribution of the energy shifts for HH and LH, and of ρ for the CB-HH transition, respectively. In Fig. 3, inset figures show the magnified data near the surface. In this calculation, we assume the SAW propagation direction to be [1-10], P_l of 200 W/m, and energy splitting between HH and LH ($\Delta E_{hh\text{-}lh}$) of 10 meV. In Figs. 3(b) and 3(c), the HH and LH energies in the absence of the strain correspond to 0 meV and −10 meV, respectively. In Fig. 3(d), ρ flips its sign around the normalized depth of 0.18, where the elliptically rotating lattice motion of the Rayleigh wave reverses its direction.

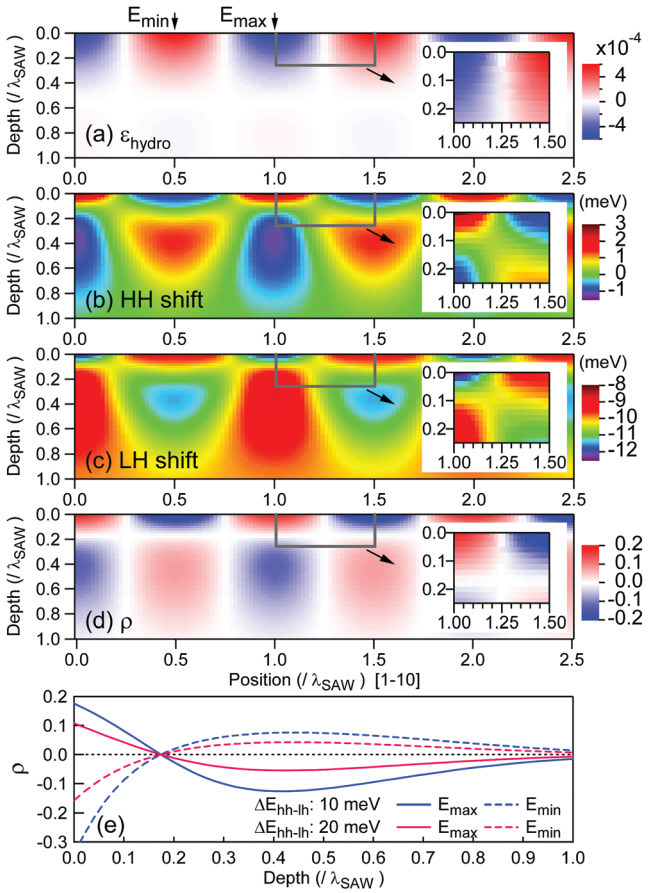

FIG. 3. (a) SAW-induced ϵ_{hydro}, (b) energy shifts of HH, (c) LH, and (d) ρ, as functions of depth and in-plane position, normalized by λ_{SAW}. (e) Depth dependence of ρ at E_{max} (solid line) and E_{min} (dashed line) for $\Delta E_{hh\text{-}lh}$ of 10 meV (blue) and 20 meV (red).

As the energy shift of the CB is proportional to $a_e\ \epsilon_{hydro}$ with a negative hydrostatic deformation potential a_e, the spatial modulation of the CB shift is sinusoidal as in Fig. 3(a) but with opposite sign. In contrast, the strain-induced HH-LH mixing affects the shifts of the HH and LH bands. As shown by the heart-shaped-like contours in Figs. 3(b) and 3(c), the lateral modulation of the HH and LH shifts deviates from a sinusoidal shape. This deviation should become less pronounced if the $\Delta E_{hh\text{-}lh}$ increases. The HH-LH interaction also modifies the characters of the HH and LH bands, and thus causing the in-plane polarization anisotropy[7] observed in Fig. 3(d). The boundaries between the positive and negative ρ areas are mainly determined by the strain distribution, while the absolute values of ρ depend on the mixing condition. Figure 3(e) shows the depth dependence of ρ at the E_{max} (solid line) and E_{min} (dashed line) positions for $\Delta E_{hh\text{-}lh}$ values of 10 meV (blue) and 20 meV (red) under the same SAW modulation. The splitting of 10 meV (20 meV) roughly corresponds to the $\Delta E_{hh\text{-}lh}$ values for QWs with $L_z = 13$ nm (9 nm), as determined from PL excitation measurements. The larger $|\rho|$ values for the smaller $\Delta E_{hh\text{-}lh}$ of 10 meV in Fig. 3(e) are attributed to the stronger HH-LH mixing compared to that for $\Delta E_{hh\text{-}lh}$ of 20 meV. Since the energy shifts of the HH and LH change the sign around the normalized depth of 0.13, $|\rho|$ values near the surface (in the deeper position) become larger for the E_{min} (E_{max}) positions, where the HH and LH come close.

We have investigated spatially resolved PL spectra and their polarization properties in GaAs/AlAs dynamic wires, which were formed by applying a SAW along the [110] or [1-10] direction on QWs. The spatial dependences of the PL modulation were found to be different for the two SAW directions. This is because the relative phases between the band gap modulation and piezoelectric modulation influence the exciton formation dynamics and thus determine the dominant emission sites. Dynamic polarization anisotropies induced by the SAW strain and their spatial dependences were also clarified. These results suggest that the polarization direction of the PL can be changed by switching the IDT applied with an electrical signal.

We gratefully acknowledge T. Tawara and S. Miyashita for fruitful discussions, comments, and for the supply of high quality samples. This work was partly supported by Grant-in-Aid for Scientific Research from the Japan Society for the Promotion of Science (19310067, 23310097).

[1]C. Weisbuch and B. Vinter, *Quantum Semiconductor Structures, Fundamentals and Applications* (Academic, San Diego, CA, 1991).
[2]J. M. Shilton, V. I. Talyanskii, M. Pepper, D. A. Ritchie, J. E. F. Frost, C. J. B. Ford, C. G. Smith, and G. A. C. Jones, J. Phys.: Condens. Matter **8**, L531 (1996).
[3]C. Rocke, S. Zimmermann, A. Wixforth, J. P. Kotthaus, G. Böhm, and G. Weimann, Phys. Rev. Lett. **78**, 4099 (1997).
[4]P. V. Santos, Appl. Phys. Lett. **74**, 4002 (1999).
[5]T. Sogawa, P. V. Santos, S. K. Zhang, S. Eshlaghi, A. D. Wieck, and K. H. Ploog, Phys. Rev. B **63**, 121307(R) (2001).
[6]F. Alsina, P. V. Santos, and R. Hey, Phys. Rev. B **65**, 193301 (2002).

[7]P. V. Santos, F. Alsina, J. A. H. Stotz, R. Hey, S. Eshlaghi, and A. D. Wieck, Phys. Rev. B **69**, 155318 (2004).
[8]F. Alsina, J. A. H. Stotz, R. Hey, and P. V. Santos, Solid State Commun. **129**, 453 (2004).
[9]T. Sogawa, H. Gotoh, Y. Hirayama, P. V. Santos, and K. H. Ploog, Appl. Phys. Lett. **91**, 141917 (2007).
[10]T. Sogawa, H. Sanada, H. Gotoh, H. Yamaguchi, S. Miyashita, and P. V. Santos, Phys. Rev. B **80**, 075304 (2009).
[11]T. Sogawa, P. V. Santos, S. K. Zhang, S. Eshlaghi, A. D. Wieck, and K. H. Ploog, Phys. Rev. Lett. **87**, 276601 (2001).
[12]J. A. H. Stotz, R. Hey, P. V. Santos, and K. H. Ploog, Nature Mater. **4**, 585 (2005).
[13]O. D. D. Couto, Jr., F. Iikawa, J. Rudolph, R. Hey, and P. V. Santos, Phys. Rev. Lett. **98**, 036603 (2007).
[14]H. Sanada, T. Sogawa, H. Gotoh, K. Onomitsu, M. Kohda, J. Nitta, and P. V. Santos, Phys. Rev. Lett. **106**, 216602 (2011).
[15]T. Sogawa, H. Sanada, H. Gotoh, H. Yamaguchi, S. Miyashita, and P. V. Santos, Jpn. J. Appl. Phys. **46**, L758 (2007).
[16]S. H. Simon, Phys. Rev. B **54**, 13878 (1996).